
INTRODUCTION

Fueled by the promise of lucrative returns, nanotechnology has enjoyed unprecedented global research and development support over the last few years. Among the many facets of this unique technology, nanomaterials appear to be the first, albeit relatively low-technology, product to have reached commercialization. Nanomaterials enjoy the advantage of an existing sophisticated microscale technology for producing bulk micropowders, fibers, and thin film in enhancing their utility as high-performance smart materials in a myriad of applications. Their unusual physicochemical characteristics are primarily governed by their very high surface area to volume ratio (or the ratio of surface atoms to the interior atoms in the cluster). Material characteristics that determine catalysis, optical properties, certain mechanical properties, and even biological phenomena generally have a length scale in the 100nm range. Nanomaterials can have very different geometries — they might be nanoparticles or clusters, nanolayers or nanofilms, nanowires, and nanodots. Building on existing robust fine-powder technology, nanoparticle materials have been among the first nanoscale products to be commercialized and are already creating a significant impact in diverse industries. These include their use in catalytic converters, oxides in sunscreens, nanoclay reinforcing fillers, abrasion-resistant oxides (e.g., alumina or zirconia-based oxides) coatings, ferrofluids, and conductive inks.

Furthermore, those materials that fall into the strict nano-regime (where one of their dimensions is <100 nm) may display unique and controllable

properties governed by quantum constraint effects (He, J. H., et al. 2007b). For instance, nanoparticles of semiconductor CdSe behave as pseudo-atoms with molecular orbitals delocalized over the entire cluster. The associated quantized energy levels¹ allow these (quantum dots) to display, on excitation, well-defined size-dependent fluorescence emissions at visible wavelengths. The bandgaps of the semiconductor nanoparticles vary with particle size. As the particle sizes of the quantum dots vary from 2 nm to 6 nm, the emission wavelength changes from blue to red when excited at $\lambda = 290$ nm. Other properties such as the ionization potential, melting temperature, catalytic activity, glass transition temperature, magnetic susceptibility are all size-dependent properties of nanomaterials.

Nanofibers, especially organic nanofibers, constitute a particularly interesting and versatile class of one-dimensional (1-D) nanomaterial. The more exotic of the conventional textile fiber technologies include “microdenier fibers” (0.2–1.5 denier per filament), produced using multistep fabrication techniques such as melt spinning using “islands at sea” type extrusion dies. Further refinement of these textile industry techniques to obtain nanoscale fibers (that are several orders of magnitude smaller in diameter) is not practical, cost-effective, or scalable. Several techniques unrelated to electrospinning were reported in early literature for the laboratory preparation of nanofibers. Self-assembly of polymers under certain conditions and drawing of polymer melts can produce small samples of polymer nanofibers.

Electrostatic spinning or electrospinning, however, remains the most convenient and scalable technique for nanofiber production. The process has been successfully scaled up and is already used in the production of industrial products such as air filter media. Fibers with a diameter in the range $d = 50\text{--}900$ nm can readily be electrospun into mats; at $d \sim 50$ nm about 10,000 polymer chains, each up to a length of 100 μm , pass through the cross-section of the nanofiber (Reneker and Chun 1996). Electrospun nanofibers are orders of magnitude smaller in diameter compared to synthetic textile fibers and common natural fibers (Table 1.1). Electrospun nanofibers with diameters as small as 3–5 nm have been reported (Zhou et al. 2003); however, these cannot be generated consistently in quantity, even at the laboratory scale. The smallest of the nanofibers, with diameters of only several nanometers, can be selected for imaging from an ensemble of nanofibers electrospun usually from dilute solutions of a high-molecular-weight polymer under carefully controlled conditions.

¹Small nanoparticles with quantized energy levels are sometimes referred to as “artificial atoms.” Although there is no central nucleus holding the electrons, a parabolic potential well holds the electrons, which can move in a two-dimensional plane in the well.

TABLE 1.1 Comparison of natural and textile fibers

Fiber	Diameter (μm)	Coefficient of Variation (%)
Spider silk	3.57	14.8
<i>Bombyx mori</i> silk	12.9	24.8
Merino wool	25.5	25.6
Human hair	89.3	17.0
Cotton	10–27	2.5
Polyester	12–25	4–5
Nylon	16–24	3–6

1.1 HISTORICAL BACKGROUND

The first documented accounts of electrostatic spinning of a polymer solution into nanofibers were described in 1902 by J. F. Cooley and by W. J. Morton (see Table 1.2). Figure 1.1 shows Cooley's diagram of the electrospinning equipment as it appears in his 1902 U.S. patent # 692,631 (note that the

TABLE 1.2 Chronological development of electrospinning patents

Year	Persons	Description
1902	Cooley, J. F.	U.S. pat. # 692,631
1902	Morton, W. J.	U.S. pat. # 705,691
1903	Cooley, J. F.	U.S. pat. # 745,276
1934–1944	Formhals, A.	U.S. pat. #s 1,975,504; 2,077,373; 2,109,333; 2,116,942; 2,123,992; 2,158,415; 2,158,416; 2,160,962; 2,187,306; 2,323,025; 2,349,950
1929	Hagiwara, K.	U.S. pat. # 1,699,615
1936	Norton, C. L.	U.S. pat. # 2,048,651
1939	Gladding, E. K.	U.S. pat. # 2,168,027
1943	Manning, F. W.	U.S. pat. # 2,336,745
1966	Simons, H. L.	U.S. pat. # 3,280,229
1976	Simm, W., et al.	U.S. pat. # 3,944,258
1977/1978	Martin, G. E., et al.	U.S. pat. # 4,043,331; 4,044,404; 4,127,706
1978	Simm, W., et al.	U.S. pat. # 4,069,026
1980	Fine, J., et al.	U.S. pat. # 4,223,101
1980/1981	Guignard, C.	U.S. pat. # 4,230,650; 4,287,139
1982	Bornat, A.	U.S. pat. # 4,323,525
1985	How, T. V.	U.S. pat. # 4,552,707
1987	Bornat, A.	U.S. pat. # 4,689,186
1989	Martin, G. E., et al.	U.S. pat. # 4,878,908
1991	Berry, J. P.	U.S. pat. # 5,024,789
2000	Scardino, F. L. and Balonis, R. J.	U.S. pat. # 6,106,913
2004	Chu, B., et al.	U.S. pat. # 6,713,011

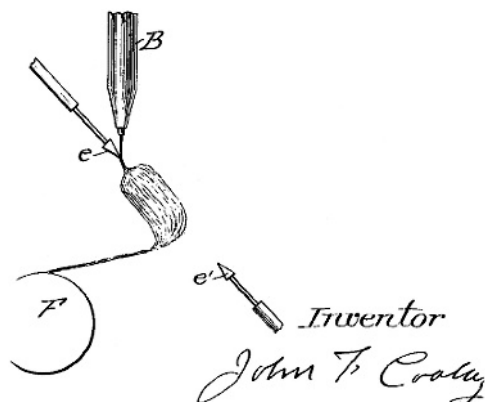


Figure 1.1 A solution of polymer (e.g., collodion or cellulose nitrate in ether or acetone) delivered into the high-voltage direct current (DC) electric field via tube *B* to form electrospun nanofibers collected on a drum *F*. (Source: Cooley 1902, Fig. 5 of U.S. patent 692, 631.)

static electricity generator connected to the electrodes is not shown).² These patents teach the deposition of a viscous polymer solution on a positively charged electrode (a roughened brass sphere) held close to an electrode of opposite charge to obtain electrostatic spinning. The spun fibers were collected as “a cob-web like mass” on the negatively charged electrode. The process was described as being the result of “electrical disruption of the fluid.” A closely related patent issued a year later in 1903 to Cooley also addressed electrospinning. The claims in the latter patent included the introduction of the viscous polymer solution near the terminus of a charged electrode, but not necessarily in contact with it, to yield electrospun fibers. These early patents emphasize the need for the polymer solution to be of adequate viscosity and used, as a specific example, the electrospinning of nitrocellulose. Interestingly, the fundamental features of the process, as described in these century-old patents, have changed little with time.

Anton Formhals, a quarter century later in 1934, patented an improved version of the electrospinning process and apparatus. His first patents on electrospinning of cellulose acetate from acetone used a fiber collection system that could be moved, allowing some degree of fiber orientation during spinning. He recognized the importance of adequate drying of the fibers prior to the nanofibers being collected on a grounded surface. By 1944, he had filed four more patents on improved processes and claimed methods to electrospin even multi-component webs that contained more than one type of nanofiber.

²The first reported electrostatic spraying of a liquid was described by Jean-Antoine Nollet in 1750, long before the term electrospaying was even coined.

In 1936, C. L. Norton (see Table 1.2) used a plate collector electrode in conjunction with a static electricity generator in his design to provide a “transverse intermittent electromotive force” to improve fiber quality and collection.

Sir Geoffrey Taylor’s contribution in the 1960s towards the fundamental understanding of the behavior of droplets placed in an electric field helped further develop the technique (Taylor 1964, 1969). In 1966, H. L. Simons (see Table 1.2) described the production of nonwoven nanofiber mats of a variety of thermoplastics including polycarbonate and polyurethane using metal grids to obtain a variety of patterned mats with uneven fiber density. His patent identifies viscosity, dielectric constant, conductivity, and volatility of the solvent as the key process parameters. His work explicitly identified the role of viscosity of the polymer solution in obtaining finer continuous fibers. Peter Baumgarten, working with an acrylic copolymer/dimethylformamide (DMF) system, described the dependence of fiber diameter on viscosity (and hence on concentration) of the solution as well as on the magnitude of the electric field (Baumgarten 1971). His experiment included a high-voltage power supply as well as a positive displacement pump.

Similar data for electrospinning polyolefins in the melt were reported by Larrondo and St. John Manley (1981a, 1981b, 1981c), with obtained fiber diameters being somewhat larger than those of solvent-spun nanofibers. Increasing the melt temperature and therefore decreasing melt viscosity resulted in smaller fiber diameters. Melt electrospinning can be an important approach, especially with common thermoplastics such as polyethylene (PE), polypropylene (PP), poly(ethylene terephthalate) (PET), and nylon (PA), which do not dissolve in common solvents (Dalton et al. 2006; Larrondo and St. John Manley 1981a, 1981b, 1981c; Lyons et al. 2004). Melt spinning, however, has to be carried out at high temperatures (usually $>200^{\circ}\text{C}$), requires larger electric fields (compared to electrospinning solutions), and is usually carried out in a vacuum.

Although this early work laid down the basic technique of electrostatic spinning, the present understanding of the process is mainly due to more recent work, especially that carried out within the last 10–15 years. Recent contributions towards understanding fluid dynamics (Hohman et al. 2001a, 2001b) and electrostatics (Shin et al. 2001a, 2001b; Spivak and Dzenis 1999) associated with electrospinning were fundamental to the resurgence of interest in the technique. Doshi and Reneker (1995), Jaeger et al. (1998) and Reneker et al. (2000) in the 1990s quantified the reduction in electrospun jet diameter as a function of distance away from the Taylor’s cone for poly(ethylene oxide) (PEO) in water. In a systematic study, Doshi and Reneker (1995) established a viscosity window for successful electrospinning of PEO solutions (applicable of course to the particular average molecular

weight of polymer used). Hayati et al. (1987) recognized the relationship between the solution conductivity and the whipping instability (as well as the likelihood of electrospray behavior). Early attempts at electrospinning polymers were beset with experimental difficulties, the most important among them being “bead” formation. Deitzel et al. (2001a), as well as Doshi and Reneker (1995), studied bead formation in nanofibers, relating their frequency of occurrence to the applied voltage and recognizing the influence of the changes in shape of droplet with electric field in yielding beaded fibers.

Present-day laboratory electrospinning equipment is quite similar to that used in the approaches described above. The basic hardware components remain the same, especially in research electrospinning apparatus. However, the availability of more stable power supply units and pulse-free pumps to regulate the delivery of polymer solution to the charged electrodes now allows for better nanofiber quality. Minor modifications to the basic experimental setup have been described. Controlling the nonlinear whipping instability during electrospinning by modifying the geometry of the applied electric fields has been attempted. Warner et al. (1999) and others (Shin et al. 2001a, 2001b), for instance, claimed to improve the uniformity of the electric field by using a disc electrode of about the same diameter as the collector at the capillary tip resulting in a parallel-plate electrode design. Others have used a second ring electrode (Jaeger et al. 1998) or auxiliary plate electrodes to control and focus the electrospun fiber on the collector plate. Using a ring electrode at the same potential as the main electrode improved stability in the initial part of the jet (close to the droplet); however, the whipping instability, which occurs closer to the fiber collection region, was not substantially improved. Most of these innovations, however, can be traced back to aspects of the very early disclosures on the technique; auxiliary electrodes and rotating collectors, and solid tips were all featured in the very earliest patents on electrospinning. For example, several early patents such as U.S. patents # 4,043,331 (1977, Martin, G. E., et al.), # 4,127,706 (1978, Martin, G. E., et al.), # 4,878,908 (1989, Martin, G. E., et al.) and # 3,994,258 (1976, Simm, W., et al.) described rotating or moving-belt type collectors for the electrospun fiber mats.

The bulk of the reported early research on electrospinning focused on a limited number of polymer/solvent combinations. Naturally, these were the polymers that were easy to electrospin under laboratory conditions. These likely included those polymers that dissolved in common solvents that are “good solvents” for the polymer, where the chain-like polymer molecules adopt open, extended macromolecular conformations (as opposed to compact globular geometries) that allow adequate entanglement of polymer chains. With potential for future scale-up in mind, solvents that are both economical and also environmentally acceptable were preferred.

These considerations encouraged water-soluble polymers such as PEO to be popularly studied in early research on electrospinning. Only limited work on electrospinning of polymers such as polyamides was reported in the early literature because of the requirement for expensive and/or hazardous solvents (e.g., formic acid for nylon-6,6).

1.2 BASIC EXPERIMENTAL APPROACH

The minimum equipment requirements for demonstration of simple electrospinning in the laboratory are as follows:

1. A viscous polymer solution or a melt.
2. An electrode (hollow tubular or solid) that is maintained in contact with the polymer solution.
3. A high-voltage DC generator connected to the electrode.³
4. A grounded or oppositely charged surface to collect the nanofibers.

Figure 1.2 is a schematic representation of the equipment generally used in laboratory electrospinning of polymer solutions.

A simple experimental setup may consist of a glass pipette drawn into a capillary at one end, carrying a few milliliters of a viscous solution of a high polymer (for example a 20% w/w solution of polystyrene (PS) dissolved in methylene chloride). The viscosity of the solution is high enough to prevent it dripping from the vertical pipette under gravity. The tube is mounted vertically a few inches (6–10 inches) above a grounded metal (e.g., aluminum) plate or drum. A metal wire electrode that dips into the solution in the tube is connected to the positive terminal of a high-voltage DC power supply unit.⁴

The power is switched on and the voltage increased to 10–20 kV using the controls on the power supply. At a certain threshold voltage (depending on a number of factors to be discussed later), a droplet of the liquid is drawn out of the tube into a cone-shaped terminus and sprays downwards

³Alternating current (AC) potentials can also be used in electrospinning. He and colleagues developed a mathematical model for electrospinning using an AC potential (He and Gong 2003; He, J.-H., et al. 2005a). A comparison of PEO mats spun from DC and AC potentials showed the latter to suppress whipping of the jet and result in better alignment of the nanofibers (Kessick et al. 2004). The charge build-up on the collector is likely to be less of a problem with AC voltage compared to DC voltage.

⁴All that is needed is a strong enough electric field, not necessarily an electrode in contact with the polymer solution. Electrospinning an 8 wt% solution of poly(acrylonitrile) (PAN) in dimethylformamide (DMF) using ionized field charging with a noncontacting ring electrode was recently reported (Kalayci et al. 2005).

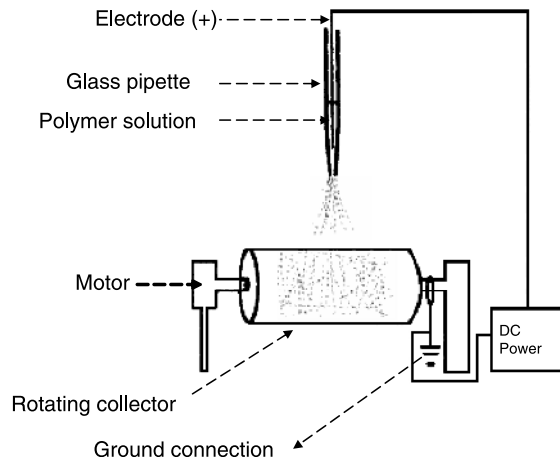


Figure 1.2 A schematic of a simple electrospinning experiment. Reprinted with permission from J.-S. Kim and Reneker (1999b). Copyright 1999. John Wiley & Sons.

as a jet towards the grounded plate as a barely visible nanoscale fiber. The high charge density on the surface of the fine jet leads to electrical instability of the electrospinning fiber, making it whip about rapidly. This splaying of the nanofiber often gives the appearance of a multiplicity of nanofibers being sprayed from the single droplet suspended from the capillary tip of the glass tube. High-speed photography, however, has demonstrated that, in general, a single nanofiber is spun out of the droplet, and its rapid movement generates the appearance of a multiplicity of fibers (Reneker et al. 2000). Consistent with this observation, one rarely observes fiber ends in high-resolution microscopic images of the nanofiber mats collected on the grounded surface. The mat is generally composed of a single long fiber arranged randomly on the collector surface. The solvent, which often accounts for more than 80% of the solution, evaporates rapidly from the surface of the spinning jet. It is desirable to select a solvent, gap distance, and temperature that would ensure that the electrospun fiber is completely dry by the time it reaches the grounded plate. Any residual surface charge on the nanofiber is rapidly dissipated on contact with the grounded metal plate, and the nanofiber mat can be peeled off it. Samples of nanofiber for microscopic examination are conveniently obtained by placing a sample collection stub over the grounded surface.

Shenoy et al. (2005a) pointed out the similarities between conventional pressure-driven dry spinning and electrospinning. Although both fiber-forming processes use polymer solutions and rely on rapid removal of the solvent to generate the fiber, the mechanisms responsible for the initial formation of the cylindrical fiber geometry and the subsequent “drawing” or thinning of the fiber are too different in the two processes to consider

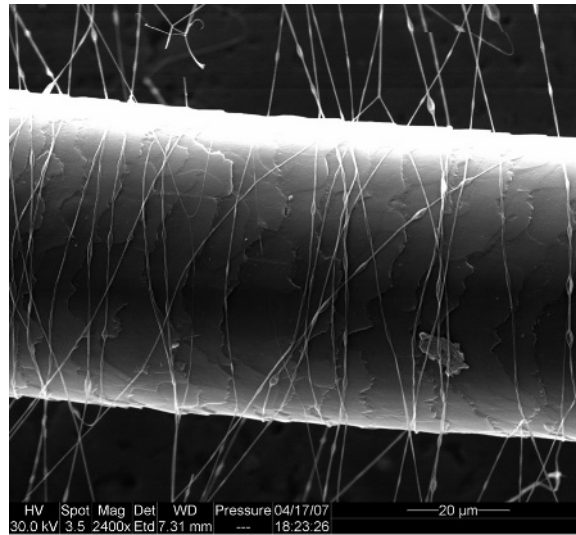


Figure 1.3 SEM image comparing the diameter of a human hair with that of PMMA nanofibers electrospun from DMF solution. (Courtesy of RTI International.)

electrospinning a special case of dry spinning. The quality of nanofibers produced in any electrospinning experiment is affected by a variety of material and process variables. From a practical standpoint, two such sets of variables might be identified — equipment-related and material-related variables. Each set includes a number of different and interrelated variables. These include the solution (or melt) temperature, concentration of solution, feed rate, electric field applied, volatility of solvent, gaseous environment about the spinning fiber, solvent vapor pressure, dielectric properties of the system, conductivity of the solution, surface tension of the solution, and the molecular weight of the polymer. These will be discussed in some detail in Chapter 4. Changing any of these can not only change fiber morphology and mat structure of the nanofiber formed, but in some instances can even determine if electrospinning occurs at all. Comprehensive predictive models that encompass all pertinent variables have not been developed as yet. Only qualitative general guidelines are available on the effect of these on fiber or mat quality, making electrospinning as much an art as it is a science.

Figure 1.3 shows a scanning electron microscopy (SEM) image of electrospun nanofibers of poly(methyl methacrylate) (PMMA) on a human hair.

1.3 DESCRIPTION OF ELECTROSTATIC SPINNING

The main features of the electrospinning process are common to electrospinning, and the former has been studied in some detail over several decades.

The differences between the two processes center on chain entanglement and the resulting elongational viscous forces that operate in polymer solutions undergoing electrospinning. This results in the extraction of a fiber, as opposed to the production of droplets, from the coulomb explosion of a supercharged drop of solution at the end of the tip or a capillary.⁵ When either a dilute solution of a polymer or solutions of a low-molecular-weight polymer are electrospun, it is common to obtain a mix of electrosprayed particles along with malformed uneven short nanofibers. Reneker and Fong (2006) separated the electrospinning process into several key stages for convenience of description: launching of the jet; elongation of the straight segment; development of whipping instability; and solidification into a fiber. The same is used here for ease of description but with the first stage subdivided into a droplet generation stage and a Taylor's cone formation stage.

1.3.1 Droplet Generation

Variants of electrospinning that do not rely on droplets being produced at the capillary or the end of a needle are known. In most laboratory studies, however, the charging of a droplet of polymer solution is the initial step in electrospinning. Typically, a polymer solution is pumped at a low flow rate into a capillary tip. In the absence of an applied electric field, the droplets form at the end of the capillary⁶ and fall off under the influence of gravity. Assuming the surface tension of the liquid, γ , and the gravitational force, F_G , to be the only two forces acting on the meniscus of the droplet, the radius of the droplet, r_0 , produced by the capillary of internal radius R is

$$r_0 = (3R\gamma/2\rho g)^{1/3}, \quad (1.1)$$

where ρ is the density of the liquid and g is the gravitational constant.

This “dripping” regime may continue even in the presence of low electric fields. When a high enough voltage is applied and the liquid has finite conductivity, the electric force F_E , as well as the gravitational force, will work against the capillary surface forces (i.e., $F_\gamma = F_E + F_G$) and the sustainable droplet size at the capillary tip will be reduced to r ($r < r_0$).

In laboratory electrostatic spraying or spinning, where a capillary⁶ carrying a positive voltage V is held at a distance L from a grounded metal surface,

⁵The term “capillary” or “tip” is preferred over the term “spinneret,” as the latter can be confused with spinnerets encountered in the spinning of textile fibers in conventional fiber manufacture.

⁶A hollow needle-like capillary is not essential for electrospinning — a droplet on a solid electrode behaves similarly. Ultrafine droplets picked up by an atomic force microscopy (AFM) tip, nanofabricated microfluidic channels (Kameoka and Craighead 2003), or by a dip-pen type tip (Sun et al. 2006) have been electrospun successfully.

F_E for the system can be expressed as in equation (1.2) (Bugarski et al. 1994; DeShon and Carson 1968; Lee 2003). The expression is based on that for an electric field at the tip of a metal point and a grounded plate as proposed by Loeb et al. (1941):

$$F_E = (4\pi\epsilon V^2)/[\ln(4L/R)^2], \quad (1.2)$$

where ϵ is the permittivity of the medium (air in most experiments) and V is the applied voltage. Bugarski et al. (1994) obtained the droplet radius r for such a system as

$$r = \{(3/2\rho g)[R\gamma - (2\epsilon V^2)/(\ln(4L/R))]\}^{1/3} \quad (1.3)$$

As V increases, r becomes progressively smaller until droplet instability sets in at a value of the electric field $V = V_C$, and electrostatic spraying occurs.

Due to the electric field, charge separation will take place in a droplet that is electrically conductive. Where the capillary is positively charged, for instance, the positively charged species migrate to the surface of the droplet and the negatively charged species accumulate in its interior until the electric field within the liquid droplet is zero. Charge separation will generate a force that is countered by the surface tension within the droplet. The velocity at which these ionic species move through the liquid is determined by the magnitude of the electric field and the ionic mobility of the species. For an electric field of $\sim 10^5$ V/m typical of electrospinning, the drift velocity has been estimated to be ~ 0.15 m/s (Reneker and Chun 1996). However, the velocity achieved by the jet itself in electrospinning tends to be much higher, reaching values of 10 m/s in typical runs. Ionic species therefore must move at comparable velocities and in the direction of the jet.

The stability of an electrically charged droplet at the end of a capillary requires the inward surface tension forces to exceed the outward repulsion forces of like charges accumulating on the droplet surface:

$$F_E \leq g\rho[(r^2/\beta) - V], \quad (1.4)$$

where g is the gravitational constant, V is the volume of the droplet, ρ is the density of the liquid, and β is the shape factor for the droplet.

However, the maximum surface charge Q_R that the surface of a droplet can accommodate in vacuum is limited by the Rayleigh condition (Rayleigh 1882):

$$Q_R = 8\pi(\epsilon\gamma r^3)^{1/2} \quad (1.5)$$

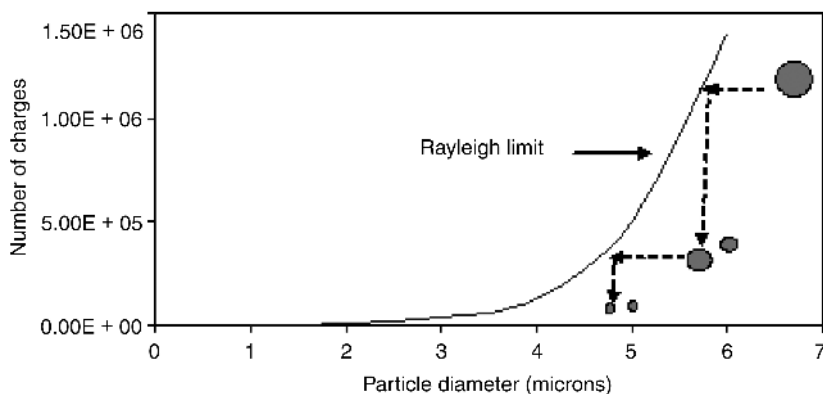


Figure 1.4 Schematic representation of the explosion of charged droplets.

At $|Q| > Q_R$ the droplet first deforms and then explodes into a number of smaller droplets due to coulombic repulsion of positive surface charges crowded on its surface. In practice, the limit can be reached by either gradually increasing the electric field or by allowing the liquid droplet under a constant electric field to reduce its diameter via evaporation. Evaporation of a charged droplet does not discernibly reduce its surface charge (Abbas and Latham 1967). However, charge transfer to ambient moisture in the spinning environment cannot be ruled out (Kalayci et al. 2005).

With low-molecular weight liquids, this build-up of electrical pressure results in primary asymmetric fission of the droplet, giving rise to smaller highly charged sibling droplets (note, spherical shape minimizes the surface) that in turn subdivide again with continued evaporation (Fig. 1.4). In the absence of long-chain polymer molecules that are long enough to undergo entanglement,⁷ break-up of the jet into individual droplets is inevitable. Under proper conditions the process may even continue until single ions result (soft electrospray ionization used in mass spectrometry and ion mobility spectrometry relies on this process to generate individual analyte ions). Negatively charged droplets will continue to disintegrate to a size where spontaneous electron emission occurs (10–100 nm depending on the value of γ). Except under very high electric fields, positive ion emission is unlikely and positively charged droplets might be expected to disintegrate down only to molecular dimensions. In addition to this fission mechanism (Dole et al. 1968), direct ion evaporation from a supercharged

⁷There are situations where other nonbonded interactions between molecules or aggregates of molecules such as micelles are strong enough to obtain electrospinning into nanofibers of solutions where no polymer is present. For example, lecithin electrospun from 35 wt% solutions in CHCl_3/DMF (70/30) was shown to yield nanofibers (McKee et al. 2006b).

droplet (Iribarne and Thompson 1976) has also been proposed. Although both mechanisms are feasible, their relative importance under various experimental conditions is not clear.

1.3.2 Taylor's Cone Formation

Deformation of relatively small charged droplets under an electric field, from a sphere to an ellipsoid, is well known (Macky 1931). The effect diminishes as r increases, because the electric field just outside the droplet varies inversely with r^2 . For droplets of water, such deformation has been observed at fields exceeding 5000 V/cm. The elongated droplet assumes a cone-like shape and a narrow jet of liquid is ejected from its point (Taylor 1964, 1969; Melcher 1972). This "Taylor's cone" is formed at the critical voltage V_C applied to a droplet at the end of a capillary of length h and radius R (Taylor 1969):

$$V_C^2 = (2L/h)^2(\ln(2h/R) - 1.5)(0.117\pi RT). \quad (1.6)$$

Observing the process in a range of different liquids, Taylor determined the equilibrium between surface tension and electrostatic forces to be achieved when the half angle of the cone was 49.3° , a value verified later by others (Larrondo and St. John Manley 1981a, 1981b). This value can, however, be different for different polymer solutions and melts. For instance, with molten PP, a half angle of 37.5° has been observed (Rangkupan and Reneker 2003). It is the change in shape of the droplet into this conical shape that defines the onset of extensional force initiating droplet/fibril formation that eventually leads to electrostatic spraying and spinning. At the minimum spraying voltage some liquids display a pulsation of the droplet, with spray being associated with these pulses. With high-viscosity liquids such as polymer solutions, a smooth transition to a Taylor's cone geometry is generally obtained. This cone-like shape is not necessarily maintained throughout the electrospinning process — it can change depending on the ratio of the feed rate to the mass transfer rate away from the droplet (Wang, Z.-G., et al. 2006). Zeleny (1935), following the work of Rayleigh, studied electrospraying from a glass capillary where the liquid was electrified (using a set of 15 Leyden jars as the generator) via an electrode. He reported multiple jets emanating from a single droplet under certain conditions. Recent high-speed imaging observations of levitated ethylene glycol droplets in an electric field showed deformation and disintegration into fine jets (often called Rayleigh jets), as predicted by Rayleigh (Duft et al. 2003). The jets disintegrated into fine droplets amounting to about 0.3% of the mass, and carrying about one-third of the total charge of the mother droplet.

Equation (1.6) suggests high-surface-tension liquids to require high electric fields V_C for electrostatic processing that may possibly lead to corona

discharge. However, neither the conductivity nor the viscosity of the liquid that forms the droplet is taken into account in the above equation or other similar expressions for V_C (Hendricks et al. 1964). In practice, however, both parameters heavily influence cone formation in electrostatic spraying and spinning and can be readily varied using additives. Although this description is based on droplet geometry, electrospinning can also occur from an essentially flat surface of liquid subjected to a strong enough electric field (Yarin and Zussman 2004).

Kalayci et al. (2005) recently described the charging process in the electrospinning solution. The mobility of an ion in the viscous solution depends upon the electrostatic force $F_E = qE$ and the viscous drag force $F_d = 6\pi\eta r' \mu E$, which work against each other (r' is the hydrodynamic radius of the ion, q is the ionic charge, η is the solution viscosity, μ is the ionic mobility, and E is the electric field strength). Their expression for the sum of electrostatic forces can be reduced to the following (Kalayci et al. 2005):

$$\begin{aligned} \sum F_{(\text{electrostatic})} &= (n_1 q E) - (n_1 6\pi\eta r'_+ \mu_+ E) - [n_1(1-y)qE] \\ &+ [n_1(1-y)6\pi\eta r'_- \mu_- E], \end{aligned} \quad (1.7)$$

where n_1 is the number of ions in a solution of mass m , $(1-y)$ is the fraction of negative ions in the droplet, and the subscripts $+$ and $-$ refer to values for the positive and negative ions. The geometric representation of the jet in the Taylor's cone area from Kalayci et al. (2005) is reproduced in Fig. 1.5. V_1 and V_2 refer to the volume of the conical frustum and the volume of the space in which the jet is contained, respectively. They assumed $V_1 = 2/3 V$ in their analysis.

1.3.3 Launching of the Jet

Due to copious entanglement of polymer chains in concentrated solution, the (outward) force available to a droplet via coulombic repulsion will generally be insufficient to explode it. However, the surface area has somehow to be increased to accommodate the charge build-up on the jet surface, and this occurs through the formation of fibers. A slender fibril emanates from the cone to create additional surface area needed to accommodate surface charges, and it initially travels directly towards the grounded collector. The effect of charge repulsion is not unlike the mechanical stretching experienced by a jet in conventional fiber spinning (Burger et al. 2006; Shenoy et al. 2005a). Studying the mobility of particles in electrospinning jets, Deitzel et al. (2006) suggested this jet initiation to occur from the surface layers of

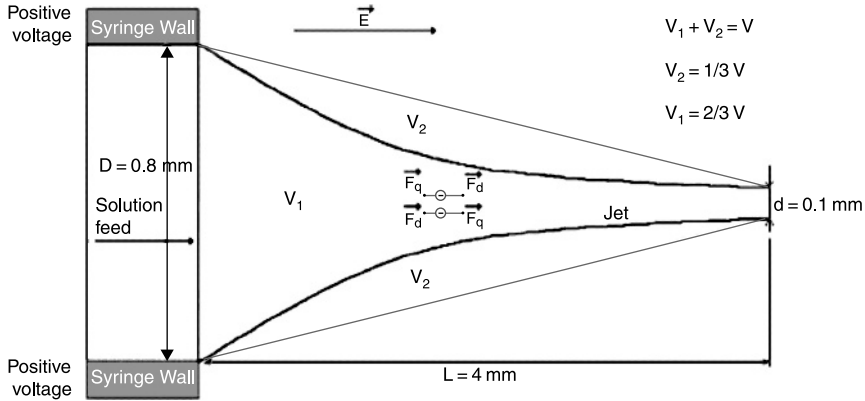


Figure 1.5 Geometric model of the Taylor’s cone region. Reprinted with permission from Kalayci et al. (2005). Copyright 2005. Elsevier.

the cone. This is partly due to surface shear forces generated by the potential difference between the base and the tip of the Taylor’s cone. Quasi-stable multiple jets emanating from the same droplet have been observed with some systems (Figs. 1.6 and 1.7). The tendency is for one of these to become stable while the others die off, without affecting the total current flow in the system (Koombhongse et al. 2001). Electrospinning a segmented polyurethane urea from DMF solutions (2.5–17% w/w) using an electric field of 6 kV/cm, Demir et al. (2002) reported as many as six jets emanating from a single droplet at low concentrations of polymer, the average number

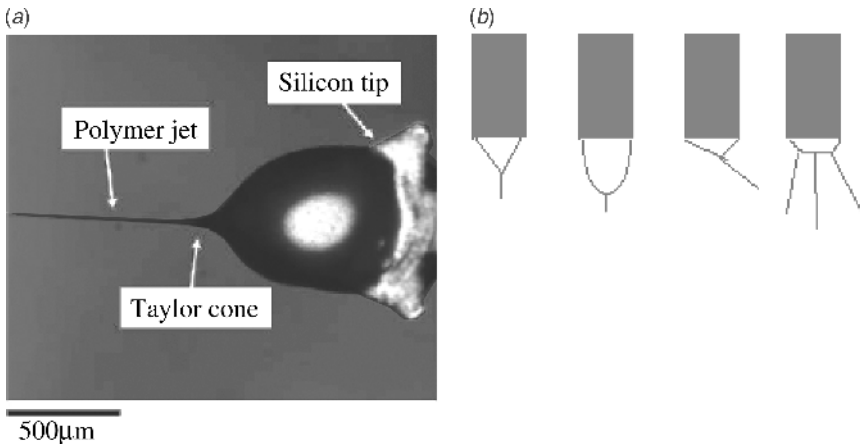


Figure 1.6 (a) Optical image of the Taylor’s cone and tapering linear segment of a jet emanating from a microfabricated silicon tip. Reprinted with permission from Kameoka et al. (2003). Copyright 2005. American Institute of Physics. (b) Diagram of different geometries of Taylor’s cone obtained in practice.

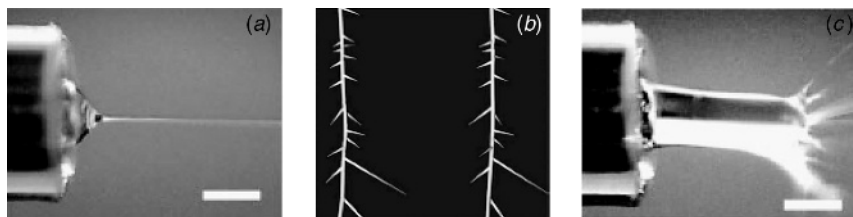


Figure 1.7 (a) Taylor's cone and straight jet formed during electrospinning of a 10 wt% solution of PLA in methylene chloride at an applied field of 1.2 kV/cm. Reprinted with permission from Larsen et al. (2004b). Copyright 2004. John Wiley & Sons. (b) Branching of jet during electrospinning captured in a high-speed photograph. Reprinted with permission from Yarin et al. (2005). Copyright 2005. American Institute of Physics. (c) Multiple jets emanating from a single elongated droplet at 1.2 kV/cm, but without N₂ flow coaxial to the jet. Reprinted with permission from Larsen et al. (2004b). Copyright 2004. John Wiley & Sons.

of jets increasing linearly with the electric field (kV/cm). Figure 1.6 illustrates the Taylor's cone.

Once launched, the jet can be described by considering the conservation of mass in the system:

$$\text{Feed rate} = (\pi d^2 \rho u)/4, \quad (1.8)$$

where $d = 2r$ is the diameter of the jet, ρ is the density, and u its velocity. Similarly, the conservation of charge for the jet yields the following (He, J.-H., et al. 2005a, 2005b):

$$\pi d Q u + (k \pi d^2 E)/4 = I, \quad (1.9)$$

where E is the applied electric field, I the current flowing through the jet, k the dimensionless conductivity of the solution, and Q is the surface charge.

1.3.4 Elongation of Straight Segment

Jet initiation occurs almost instantaneously on application of a voltage exceeding V_C to the polymer solution. The coulombic repulsion of surface charges on the jet has an axial component that elongates the jet in its passage towards the collector. Laser doppler velocimetry experiments (Buer et al. 2001) reveal the velocity of the jet as well as the variance in jet velocity to increase with the distance away from the Taylor's cone. As a result, the jet diameter decreases rapidly due to both extension and evaporation of the solvent. The initially straight jet tapers down as it accelerates towards the collector, and the tapering is pronounced in the region below the Taylor's cone. As the jet thins, the

surface area per unit mass of jet material increases while the surface charge per unit area decreases. Loss of charge by adventitious discharges due to air-borne charged species and ions, which neutralize the surface charge on the fibers, become increasingly likely as the surface area increases. However, solvent evaporation continually increases the surface charge per unit area, driving the increase in surface area through extension.

It is the extensional modulus of the rapidly drying jet (due to chain entanglement) that prevents the onset of capillary instability and yields a stable jet. Recent work on electrospinning of PEO solutions containing low-molecular-weight poly(ethylene glycol) (PEG) emphasizes the role of elasticity of the jet in obtaining electrospinning (Yu et al. 2006). For these systems the ratio of the fluid relaxation time to the time for growth of instabilities (the Deborah number) was shown to correlate with arrest of Raleigh instability and with electrospinning. Bunyan et al. (2006) reported the length of the linear jet to increase when the electric field was changed by increasing the diameter of the collector disc electrode used at the spinneret.

Xu and Reneker (2006) measured the diameter of spinning jet at different points below the Taylor's cone using interference colors generated when a beam of light impinges on the jet. The technique allows diameters in the range of 500 nm to 15 μm to be conveniently measured in real time using a single camera and a light source. The diameters can also be measured by laser velocimetry (Warner et al. 1999) or by optical imaging near the Taylor's cone (Deitzel et al. 2006), but the procedure becomes increasingly difficult when nanofiber diameters taper down to dimensions close to the wavelengths of light. As the jet diameters dip below 100 nm, very significant chain orientation (made evident by changes in birefringence) occurs. The relative modulus at the surface of electrospun nanofibers was recently measured using scanning probe microscopy (SPM) techniques (Ji et al. 2006b), and was found to increase with the decrease in fiber diameter. This is likely due to the shear-induced orientation of chains (Jaeger et al. 1996). The length of the linear portion of the jet, as well as the rate at which its diameter is reduced due to drawing, is determined by the solution feed rate and the strength of the electric field. It is useful to learn the composition of the jet at different distances from the Taylor's cone to be able to quantify the drying rate of the jet. Raman spectroscopy has been successfully used (although only on relatively thick jets) to obtain a polymer : solvent ratio in the electrospinning jet (Stephens et al. 2001).

Modeling the behavior of a jet in this linear regime, before the onset of whipping, appears to be relatively straightforward and has been attempted (Feng 2003). Experimental results appear to be in reasonable agreement with the models. The simpler one-dimensional models that assume the solution to be a leaky dielectric provide good numerical dimensions of

the jet in this region (Hohman et al. 2001a, 2001b). Recently, J. H. He et al. (2005a, 2005b) used a simple approach based on Cauchy's inequality to model the straight region of the jet and to predict the length L of the jet segment.

1.3.5 Whipping Instability Region

The initially straight jet segment invariably becomes unstable and displays bending, undulating movements during its passage towards the collector. Early-stage varicose instability that promotes jet extension to accommodate surface charges can be modeled reasonably well. Bending of the jet invariably increases surface area and therefore tends to reduce the density of charges. Theoretical studies on electrically forced jets by Hohman et al. (2001b), Reneker et al. (2000), Yarin et al. (2001a, 2001b), and others (Spivak and Dzenis 1998; Spivak et al. 2000) modeled the whipping jet as being the result of competition between several different modes of instability. These modes of instability (that incidentally also occur in nonviscoelastic solutions) are Raleigh instability, axissymmetric instability, and bending mode instability (Shin et al. 2001a, 2001b). The mode of instability obtained is dependent on the electric field, with stronger fields favoring whipping instability. The jet in this region exhibits components of electrostatic repulsive forces that are not predominantly axial (Hohman et al. 2001b). As a result, it whips about within a conical envelope, still symmetrically arranged about the axis of its straight segment. Figure 1.8 shows an image of the whipping region of a jet and also illustrates two modes of instability in the jet. It is the whipping instability that dramatically increases the surface area of the jet and rapidly lowers the surface charge density.

High-speed imaging studies of the jet by Reneker et al. (2000) concluded the jet to be invariably thrown into a series of loops of increasing diameter, spiraling down towards the collector. The cone-shaped envelope of the unstable jet typical of electrospinning is created by the rapid symmetric movement of a single jet. The axis of the straight jet is maintained and the additional envelope volume that contributes to the loops of larger diameter is generated via extension of the jet along the perimeter of the loops. Reneker's images of larger loops closer to the collector show higher order bending instability where the jet being looped forms right- and left-handed coils (Reneker et al. 2000). Both the rate of increase in surface area during whipping instability and the solvent evaporation rate are high in this regime, further reducing the jet diameter. Interplay between the increasing charge density on the one hand, and the viscous and surface tension forces that resist elongation on the other determines the intricacies of the instability obtained. Even more complicated modes of whipping instability resulting in particularly complex curved

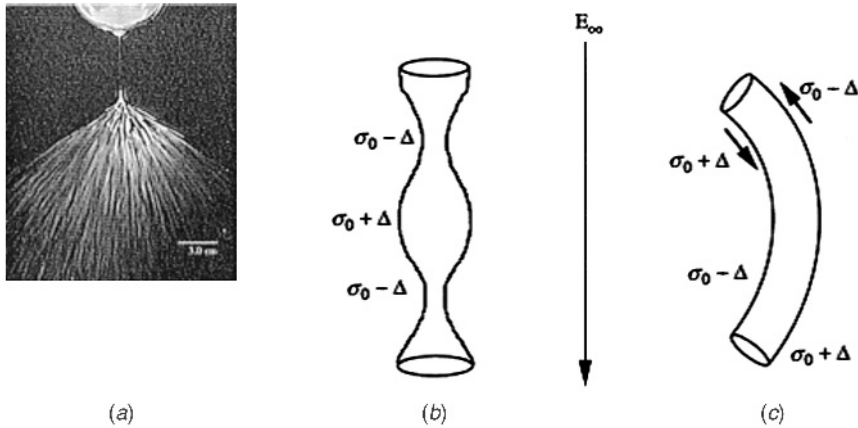


Figure 1.8 (a) Image illustrating the whipping region of a typical electrospinning jet (Reneker et al. 2000). (b) Axisymmetric instability and (c) bending instability in a fluid jet carrying a surface charge, placed in an electric field. Reprinted with permission from Shin et al. (2001b). Copyright 2001. Elsevier. $\Delta\sigma$ denotes the perturbation of the surface charge density and arrows indicate the direction of local torque responsible for bending.

trajectories of electrospinning jets have been observed in practice (Reneker et al. 2002).

From the above description it is clear that whipping instability is the primary mechanism responsible for reducing nanofiber dimensions during electrospinning. However, as Dzenis (2004) pointed out recently, suppressing this instability using either a secondary electric field or a short gap distance (between the tip of the needle and the collector) did not result in substantially thick nanofibers being generated. Understanding of the process is incomplete, and all the factors that govern fiber formation are not well understood.

Whipping instability is a rapid process and it is possible for surface charges to be nonuniformly distributed and to result in sections with high local charge density. This may give rise to secondary jet initiation, resulting in the formation of somewhat less frequent branched nanofibers (see Fig. 1.7b) (Yarin et al. 2005). Branching allows a means of rapidly increasing surface area to accommodate local concentrations of charges. Initiation of such splaying (Deitzel et al. 2001a; Fang and Reneker 1997; Hsu and Shivkumar 2004a, 2004b) and the presence of branched fibers in mats have been observed in practice (Koomhongse et al. 2001; Krishnappa et al. 2003). Inducing splaying by using co-solvents of higher conductivity and/or dielectric constant can therefore result in smaller average fiber diameters as observed for poly(ϵ -caprolactone) (PCL) in CHCl_3/DMF system (Hsu and Shivkumar 2004b; Lee et al. 2003b).

Deitzel et al. (2001a) attributed the presence of smaller-diameter nanofibers in the bimodal distribution of fibers from electrospinning PEO in water solutions to splaying of the jet.

It is useful to review the different forces acting on the whipping charged jet during electrospinning (Wannatong et al. 2004):

1. Gravitational force F_G (towards the collector plate in a vertically arranged apparatus). The force is dependent on density of solution (usually ignored in models). $F_G = \rho\pi r^2 g$, where ρ is the density of the liquid and g is the acceleration due to gravity.
2. The electrostatic force F_E , which extends the jet and propels it towards the grounded collector. The force is determined by the applied electric field and material characteristics. $F_E \propto E$.
3. Coulombic repulsion forces F_C on the surface of the jet, which introduce instability and whipping motions. The magnitude of F_C is dependent on the characteristics of the polymer and solvent.
4. Viscoelastic forces, which work against elongation of the jet in the electric field. This depends on the polymer molecular weight, the solvent, and the type of polymer.
5. Surface tension forces, which work against the stretching of the jet. This depends on solvent type, polymer, and additives.
6. Frictional forces between the surface of the jet and the surrounding air or gas.

The interplay of these different forces (a simple expression is the sum of these forces) determines the diameter of the jet. Some of these change very rapidly in time due to solvent evaporation and charge dissipation, making any quantitative description of the process particularly difficult. Consequently, no entirely satisfactory mathematical models describing jets undergoing whipping instability are available.

Models that are applicable to the onset of instability in the linear instability region are available and primarily interpret instability in terms of surface charge density, viscosity, and inertia. Particularly interesting would be models that accurately predict the envelope of the undulating or whipping nanofiber as well as its change in diameter with time. Fridrikh et al. (2003, 2006) developed a model of the nonlinear behavior of jets in electrospinning of non-Newtonian fluids. Their model takes strain-hardening also into account and suggests that during the later stages a terminal amplitude for the instability and a corresponding terminal jet radius, h_f , are reached by the jet (provided the gap length is sufficiently large). Despite approximations used in their model to account for drying of the jet, agreement between experimental data (on electrospinning PCL solutions) and model predictions on the

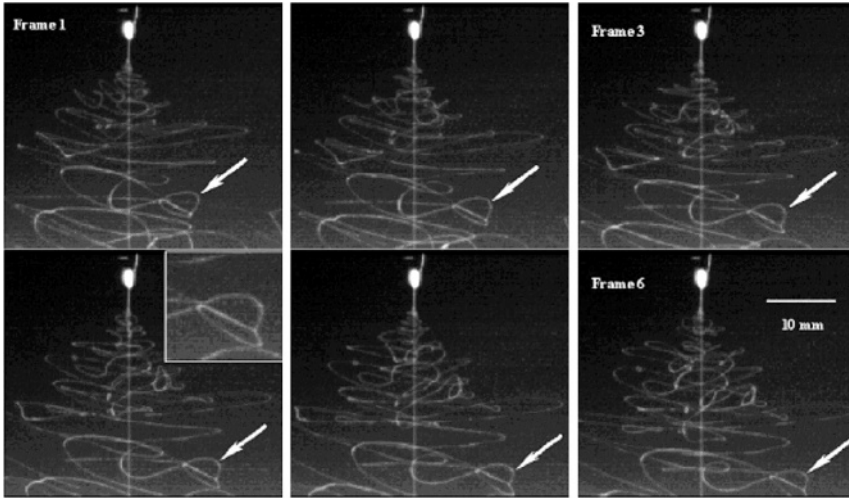


Figure 1.9 Complicated trajectories of the jet in the whipping instability region during the electrospinning of PCL in 15 wt% acetone solution (applied voltage is 5 kV and gap distance is 14 cm). Reprinted with permission from Reneker et al. (2002). Copyright 2002. Elsevier.

dependence of h_f on the inverse charge density of the jet, Σ^{-1} , are impressive. The scaling $h_f \approx \Sigma^{-2/3}$ appears to hold, at least for the narrow range of fiber diameters for which data are available. Figure 1.9 shows the complex jet trajectories obtained in whipping instability.

The high strain rate experienced by the jet results in a degree of polymer chain orientation in the nanofibers. High axial strain rates of about $10^5/s$ expected (Reneker et al. 2000) in electrospinning should be sufficient to extend the conformations of polymers with even the shortest relaxation times. Although this elongation of the jet is sufficient to induce a considerable degree of chain orientation in the polymer nanofiber, it is generally not expected to result in any chemical degradation by chain scission. Gel permeation chromatographic (GPC) studies on PS before and after electrospinning from tetrahydrofuran (THF) solutions did not show a significant difference in molecular weight (Casper et al. 2004).

Often, the jet dries too rapidly to allow extensive crystallization, but some orientation can still result. With PEO electrospun from a 10 wt% water solution, X-ray studies (WAXD pattern) shows broad diffused peaks as opposed to characteristic powder patterns for the polymer (Deitzel et al. 2001b, 2001c). The effect of macromolecular strain on the secondary structure of the nanofiber is particularly important in processing biological polymers. Changes in secondary and tertiary structure in biopolymers can result in corresponding loss of activity. Nylon-6 and nylon-12 electrospun from 15 wt%

HFP solutions when investigated using Raman spectroscopy showed evidence of changes in macromolecular conformation due to electrospinning (see also Chapter 6). In the case of nylon-6, the crystalline structure changed from the α -form to the γ -form, implying high strain on the fibers during their formation (Stephens et al. 2004). The conformation of macromolecules and the type of crystallinity obtained in electrospun fibers are therefore different from those in cast films of identical material (Stephens et al. 2005).

1.3.6 Solidification into Nanofiber

The duration available to the jet to undergo whipping instability is also governed by the rate of evaporation of the solvent, which occurs at increasing rates on a mass basis as the jet area dramatically increases during whipping. With a solvent of high vapor pressure, the elongational viscosity of the jet may reach levels too high to achieve any further deformation quite early in the whipping instability stage, yielding thick nanofibers. Solvent volatility is therefore a key consideration in controlling fiber diameter. With appropriate selection of solvents and process parameters, extremely fine nanofibers⁸ can be electrospun. For instance, increasing the volume fraction of the less volatile DMF in a THF/DMF solvent mixture yielded decreasing nanofiber diameters for electrospinning of PVC solutions (Lee, K. H., et al. 2002). As reported for the case of PS (Megelski et al. 2002) and PC/polybutadiene blends electrospun from THF/DMF (Wei et al. 2006a), the microstructure of the nanofibers and hence their mechanical integrity is also governed by the volatility characteristics of the solvent mixture. A quasi-one-dimensional model that describes

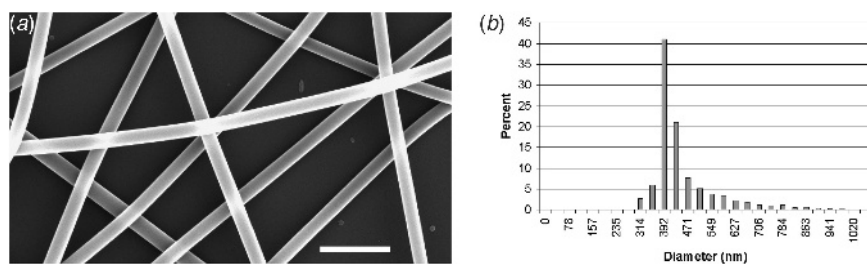


Figure 1.10 (a) Scanning electron micrograph of PS nanofibers electrospun from a 22.5 wt% solution in DMF using a 0.15-mm diameter Teflon tube as the capillary tip. Scale bar is 2 μ m. (b) Nanofiber diameter distribution derived from the image. (Courtesy of RTI International.)

⁸Nanofibers with diameters in the 1–2 nm range have been electrospun from solutions of nylon (Huang, C. B., et al. 2006a). Burger et al. (2006) estimated that a nanofiber 100 nm in diameter stretched from the Earth to the Moon (a distance of 380,000 km) would have a mass of only \sim 3 g.

the volume change in the jet and incorporates evaporation has been proposed (Yarin et al. 2001a). However, the models presently available do not fully take into account the kinetics of drying of the nanofiber and the consequent changes in rheology that affect the finer dimensions and deposit patterns.

The fibers obtained under the best electrospinning conditions are generally of circular cross-section, continuous, and bead free. However, the literature on electrospinning reports other geometries of nanofibers (Koombhongse et al. 2001; Larsen et al. 2004a; Reneker et al. 2002). Figure 1.10 show defect-free nanofibers of PS electrospun from methylene chloride solution.

1.4 NANOFIBER APPLICATION AREAS

Nanofiber-related publications and patents appear to have grown in number rapidly over recent years. An analysis of patent activity in particular allows an overall summary of the commercial potential of electrospun nanofibers and affords the identification of application areas where the technology might play a key role. A large majority of the patents issued on the technology are U.S. patents, with about two-thirds being related to biological or medical application of nanofibers. The second largest group deals with application of nanofibers in filtration, followed by other applications such as sensors, composites, and catalysis. Figure 1.11 by Huang et al. (2003) illustrates the diversity of applications where nanofibers might be used.

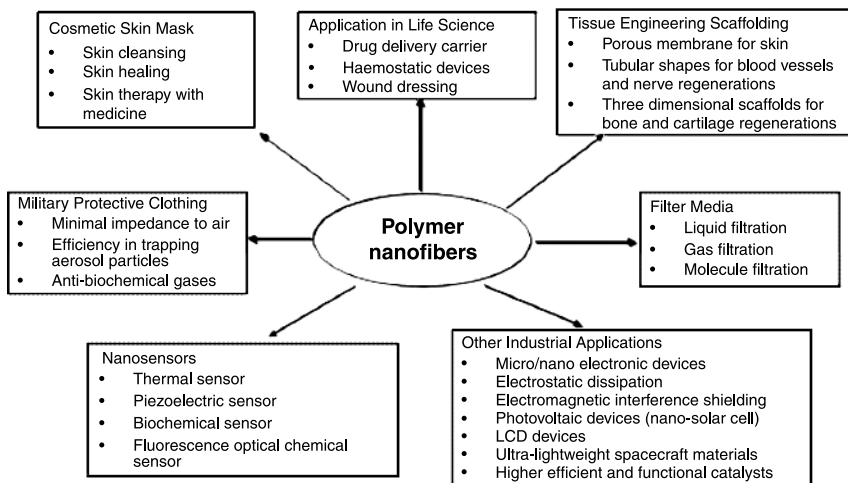


Figure 1.11 The diversity of applications proposed for polymer nanofibers. Redrawn with permission from Huang et al. (2003). Copyright 2003. Elsevier.

The following discussion identifies the major application areas for nanofibers reported in the literature. However, numerous examples of other possible applications such as magnetoresponsive fiber materials (Li, D., et al. 2003a; Tan, S. T., et al. 2005; Wang, M., et al. 2004b; Zhu et al. 2006b), electrical applications such as carbon nanofiber-based supercapacitors (Kim and Yang 2003; Kim, C. et al. 2004a, 2004c, 2004e; Kim, C., 2005), nanofiber photovoltaic devices (Drew et al. 2002; Onozuka et al. 2006; Tomer et al. 2005), catalysis applications (Demir et al. 2004; He and Gong 2003; Li, D., et al. 2004b; Wang, Z.-G., et al. 2006), and superhydrophobic surfaces (Acatay et al. 2004; Jiang, L., et al. 2004; Ma, M. L., et al. 2005a, 2005b; Singh et al. 2005; Ying et al. 2006; Zhu et al. 2006c) have been reported in the literature.

1.4.1 Filtration and Protective Apparel

As the efficiency of particle capture in an air filter increases with decreasing fiber diameter in a mat, using nanofiber filters for air or gas filtration (Liu and Rubow 1986; Park and Park 2005; Qin and Wang 2006) as well as in liquid filtration (Shin et al. 2005; Wang, X. F., et al. 2005; Yoon et al. 2006) are promising applications. The very low resistance to air flow afforded by nanofiber mats makes them especially good candidates as filter media. Commercial air-filter manufacturers such as Donaldson Inc. (Minneapolis, MN) have developed the technology for well over two decades. In recent years, several key patents claiming constructs where nanofibers are integrated with conventional filter media have been issued to Donaldson Inc. Using nanofibers in conjunction with (e.g., formed on the surface of) conventional filter media as described in these patents offers a practical advantage because of the relative fragility and difficulty of handling unsupported polymer nanofibers. Donaldson's Ultra-Web[®] nanofiber filters, commercialized in 1981, are used in industrial air cleaning. With the U.S. air-filter market alone estimated at \$7.5 billion (estimate by the McIlvaine Company, November 2005), there is continued corporate interest in filtration applications. The need for low-cost, high-efficiency particulate air filters (HEPA-grade) for the homeland security and military markets also contributes to the growth of nanofibers filter development now and in the coming years.

Demand for light-weight protective apparel for military personnel has helped the development of nanofiber materials for future textile applications (Gibson and Schreuder-Gibson 2000, 2006; Schreuder-Gibson et al. 2002; Tsai et al. 2002). These require high permeability to moisture and gases to ensure the breathability of the fabric, and should be able to effectively filter out biological particles and ultrafines in air. Nanofibers may in principle be used alone or in combination with other nonwoven materials for protective garments. High-strength and high-temperature nanofibers will be particularly

appealing in this particular application (Huang, C. B., et al. 2006b). Also of interest will be reactive textile fibers that carry specific additives that interact with chemical threat agents in air [e.g., the nanosized MgO filler to remove organophosphorous agents (Ramaseshan et al. 2006)]. These may offer a substitute for the currently used garments based on charcoal absorption technology. Nanocrystalline (magnesium oxide–PEO) composite nanofibers have been reported by Ramkumar and colleagues (Subbiah et al. 2005) to be effective against nerve agents (Sarin, Soman, and VX agents) as well as organophosphorous agents. Nanocrystalline magnesium oxide is particularly effective as a destructive adsorbent, breaking P–O and P–F bonds and immobilizing the resultant fragments (Gibson et al. 1999; Hussain et al. 2005). Poly(vinyl pyrrolidone) (PVP) nanofibers filled with oxides of tungsten and molybdenum have been investigated as gas sensor elements (Sawicka et al. 2005). Highly porous nanofiber mats and their potential for chemical modification via their high surface area therefore make them particularly good candidates for the application (see also Chapter 8).

1.4.2 Tissue Scaffolding and Drug Delivery

There is a growing need for bioresorbable three-dimensional tissue scaffolding matrices (Murugan and Ramakrishna 2006; Yoshimoto et al. 2003; Zhang, Y. Z., et al. 2005a; Zong et al. 2005), for artificial organ design (Venugopal and Ramakrishna 2005; Zhong et al. 2006), and as drug delivery platforms for therapeutic agents (Luu et al. 2003; Zeng et al. 2003b; Zhang, C. X., et al. 2005a) such as peptides and nucleic acids. Both application areas find the very high specific surface area of nanofibers to be an advantage in designing the next generation of devices. The finding that biodegradable polymers can be electrospun into nanofibers and that different cell types have been shown to adhere and proliferate on the fibrous scaffolding encourages applications research in this area. Particularly exciting is the finding that mammalian stem cells survive and proliferate on the nanofiber surfaces (see also Chapter 7).

1.4.3 Nanocomposites

The use of reinforcing fillers and fibers in polymers to improve their mechanical properties is commonly encountered in polymer technology. Conventional fibers such as carbon fibers, glass fibers, gel-spun polyethylene fibers, and aramids are routinely used in composites of a range of different polymers (Chronakis 2005). The improvement in modulus and strength achieved by using even low levels of a reinforcing fiber in a composite is impressive. Some of this improvement is due to the properties at the fiber/matrix interface and therefore dependent on the surface area of the

interface. Nanofibers, with their very high specific surface area, should therefore deliver particularly good composite characteristics. For instance (poly(2,2'(m-phenylene)-5,5'-dibenzimidazole)) (PBI) electrospun nanofiber filler in epoxy EPON 828 (Shell Chemical Company) and rubber matrices has been studied by Kim and Reneker (1999a). Even at the 10 phr level, the nanofibers increased the modulus of styrene-butadiene rubber (SBR) tenfold! Nanofibers of nylon-4,6 used in an epoxy matrix that yielded a transparent composite have also been reported (Bergshoef and Vancso 1999). This book does not include a detailed discussion of nanofiber-filled polymer composites; most of the published work on the topic appears to deal with the use of carbon nanofibers and nanotubes as fillers. However, Chapter 6 discusses composite nanofibers (electrospun or post-treated to yield nanofibers made up of polymer/filler materials).

1.4.4 Sensor Applications

Nanofibers are attractive sensor materials because their high specific area allows them to sorb and/or react rapidly with low levels of analytes in the air (Aussawasathien et al. 2005; Dersch et al. 2005; Ding et al. 2005b; Virji et al. 2004). It is reasonable to therefore expect better performance from nanofiber sensors. Examples of chemical sensors based on a change in electrical resistance have recently been reported. For instance, using nanofibers (~ 100 nm) of polyaniline (PANI), several workers were able to detect NH_3 levels down to 0.5 ppm (Liu et al. 2004). Generally, the nanofiber geometry appears to improve sensitivity as well as the response time of chemical sensors compared to similar chemistries used in thin-film geometries (see also Chapter 8).